Original paper
Biomechan Model Mechanobiol 2 (2004) 205–217 © Springer-Verlag 2004
DOI 10.1007/s10237-004-0039-6

Stainless and shape memory alloy coronary stents: a computational study on the interaction with the vascular wall

Francesco Migliavacca, Lorenza Petrini, Paolo Massarotti, Silvia Schievano, Ferdinando Auricchio, Gabriele Dubini

Abstract Balloon-expandable and self-expandable stents are the two types of coronary stents available. Basically, they differ in the modality of expansion. The present study analyses the stress state induced on the vascular wall, by the expansion of balloon- and self-expandable stents, using the finite element method. Indeed, modified mechanical stress state is in part responsible in the restenosis process. The balloon-expandable stents herein investigated are assumed to be made of stainless steel, while the self-expandable stents are made of a shape memory alloy. The effects of the severity of the coronary stenosis, the atherosclerotic plaque stiffness and the stent design are investigated. Comparing the self-expandable stent with the balloon-expandable one, the former induces fewer stresses and lower damage to the vessel, but, on the other hand, its lower stiffness induces a lower capability to restore vasal lumen and to contrast arterial elastic recoil.

1 Introduction

A vascular stent is a small metal tube, which is inserted into an artery at the site of a narrowing to act as internal scaffolding or as a support to the blood vessel. Two types of coronary stents are available on the market based on two different expansion principles: the balloon-expandable and the self-expandable stent. The former is mounted on a catheter supporting a balloon and is positioned by inflating the balloon in the site of blockage. Under the pressure of the balloon, the stent deploys itself to mechanically support the vessel wall. When the balloon is deflated and retracted, the stent remains in place and keeps the artery open. On the other hand, the self-expandable stent is mounted on a catheter and then compressed by a protective sheath. When the sheath is retracted the stent expands by itself into the artery. In both cases, in the weeks following the insertion of the stent, a thin film of cells grows over the metallic frame lining the walls of the artery like a skin. Until the skin has grown over the metal there is a risk for blood elements to stick to the stent. This is a phase of the in-stent restenosis process, which includes an inflammatory phase, a granulation or cellular proliferation

Received: 1 September 2003 / Accepted: 29 December 2003
Published online: 17 March 2004

F. Migliavacca
Dipartimento di Bioingegneria,
Politecnico di Milano, Milan, Italy

G. Dubini
Dipartimento di Ingegneria Strutturale,
Politecnico di Milano, Milan, Italy

F. Migliavacca (✉), P. Massarotti, S. Schievano, G. Dubini
Laboratory of Biological Structure Mechanics (LaBS),
Politecnico di Milano, Piazza Leonardo da Vinci 32,
20133 Milan, Italy
E-mail: francesco.migliavacca@polimi.it
Tel.: +39-02-23994283
Fax: +39-02-23994286

L. Petrini, P. Massarotti, S. Schievano, F. Auricchio,
Dipartimento di Meccanica Strutturale,
Università degli Studi di Pavia, Italy

Financial support from the Italian Ministry of Education, University and Research (MIUR) is acknowledged.

phase, and a phase of remodeling involving extracellular matrix protein synthesis. It is worthwhile noting that the restenosis is also present after an intervention of angioplasty, but there are profound differences between vascular biological responses to balloon- and stent-induced injury (Welt and Rogers 2002). If compared to angioplasty, stenting improves the short-term success rate and the safety of the percutaneous coronary intervention. In the longer term, it decreases the restenosis and the need for repeated revascularization. However, stenting does not eliminate restenosis. The three major pathogenic factors in restenosis are arterial elastic recoil, negative arterial remodeling, which is an effect of adventitial thickening resulting in vessel shrinkage (Mintz et al. 1997; Schwartz et al. 1998; Sangiorgi et al. 1999), and neointimal hyperplasia. Stents virtually eliminate elastic recoil and counteract the arterial remodeling, but neointimal hyperplasia after stenting can still cause significant and refractory restenosis (Schwartz and Henry 2002).

Intravascular brachytherapy has been used in recent years and been found to be effective in managing in-stent restenosis, but the recurrence after brachytherapy is still significant (Leon et al. 2001; Popma et al. 2002; Waksman et al. 2002). Similarly, stent-based drug delivery has been developed in an attempt to counteract the restenosis phenomenon. A number of drugs have been studied and additional ones are being pursued at present: anticoagulants (heparin, hirudin), antiplatelet agents (abciximab), anti-inflammatory drugs (dexamethasone), and antiproliferative agents (sirolimus, paclitaxel, actinomycin D and batimastat). To date, the sirolimus-eluting stents demonstrate remarkable efficacy and safety in preventing restenosis (Sousa et al. 2001; Morice et al. 2002, Degertekin et al. 2003).

The process of neointimal hyperplasia initiates from the arterial injury sustained during percutaneous coronary intervention. Edelman and Rogers (1998) described the four phases of the vascular response to endovascular implants: thrombosis, inflammation, proliferation and later remodeling. Indeed, the thrombus that forms in the vicinity of the stent struts following the arterial injury and intimal denudation activate the inflammatory responses. Growth factors and produced cytokines would activate proliferation and migration of smooth muscle cell and allow production of extracellular matrix. Together these processes significantly limit intra-arterial lumen leading to restenosis. These observations support the notion that wall stress is a potent stimulus for pathophysiological adaptations of the vessel wall. As a consequence the knowledge of the stress state generated during the intervention may help in understanding some aspects of the restenotic process, which could be as one of the outcome of a modified mechanical stress state. It is well known, indeed, that atherosclerotic lesions occur where there are local variations in the arterial mechanical and fluid dynamics environments (Zarins et al. 1983; Gibson et al. 1993; Bassiouny et al. 1994; Thubrikar and Robicsek 1995; Gnasso et al. 1997; Saul 1999; Jiang et al. 1999, 2000; Feldman and Stone 2000; Wentzel et al. 2003). The outward force of the stent against the vessel wall creates non-physiologic stresses and strains. The initial induced process is an acute elasto-damage with abnormal stresses, followed by a stress-mediate injury response. In this light, the stent design as well as the modality of stent expansion could produce a different arterial response to the mechanical action induced by the stent itself. The mechanical stresses produced during the expansion should be reduced as much as possible not to hinder the beneficial effects of the treatment.

Although the drug eluting stent implantation seems to prevent restenosis (Degertekin et al. 2003) better than the bare stents and appears up to now as the best solution available, the mechanical injury to the vessels is still not eliminated. In this context, the present study, which does not address the topics of drug diffusion into the vessel wall as well as the convective transport in the blood stream, is still meaningful. Indeed, stress-strain analysis, force and tension calculations are important parameters by which evaluate the response to these implants (Edelman and Rogers 1998, Moore and Berry 2002).

In the scientific literature there has been an increasing effort to study angioplasty and stenting procedures by means of computational structural analysis (Lee et al. 1993; Oh et al. 1994; Rogers et al. 1999; Gourisankaran et al. 2000; Auricchio et al. 2001; Holzapfel et al. 2002, Prendergast et al. 2003) with the aim of predicting and calculating the stress state generated after a percutaneous coronary intervention. In particular, the work by Holzapfel et al. (2002) is one of the most exhaustive on the subject and we refer the reader to this reference since it also contains a brief review of the other studies mentioned.

The present work is inserted in the computational field and aims to investigate the stress state induced on the vascular wall by the expansion of 1) a stainless steel and 2) a shape memory alloy stent using the finite element method (FEM). In particular, the radial force produced on the vascular wall responsible for the lumen enlargement and the circumferential stress are analyzed in detail. Furthermore, the effects of the severity of the coronary stenosis as well as of the stiffness of the atherosclerotic plaque are investigated.

2
Materials and methods

In this work a numerical study of coronary stent expansion and contact with an atherosclerotic vessel is proposed. In particular the geometry of a well-known commercial stainless steel stent is adopted. A parametric analysis varying the stiffness of the atherosclerotic plaque, the severity of the vascular stenosis, the metal-to-artery surface ratio and the material of the stent (stainless steel (SS) and shape memory alloy (SMA)) is carried out. Finally, the methodology herewith described is also used to study the deployment of a new-generation self-expandable stent design.

Large deformation analyses are performed using the FEM commercial code ABAQUS/Standard 6.2 (Hibbit Karlsson & Sorenses, Inc., Pawtucket, RI, USA).

2.1
The stainless coronary stent expansion

The 3-D model considered in this study is depicted in Fig. 1. It consists of three parts: the stent, the artery and the atherosclerotic plaque. Due to the model symmetries only one twelfth is reproduced in the circumferential direction and one half in the longitudinal one.

The stent model is the one adopted in a previous study (Migliavacca et al. 2002) and reproduces the typical diamond-shaped intravascular stent (Palmaz-Schatz). In its unexpanded configuration, it is assumed to be a tube with rectangular slots on its surface. The dimensions are as follows: the whole stent has a length of 16 mm, an outer diameter of 1.2 mm, a thickness of 0.1 mm, 5 slots in the longitudinal direction and 12 slots in the circumferential direction; each slot has a length of 2.88 mm, and a metal-to-artery surface ratio (m/a) of 0.17, which is the ratio of the actual metal surface in contact (m) and the arterial wall surface (a). The stent is discretized by means of 1124 10-node tetrahedral elements with a corresponding number of nodes of 2760. The stent is assumed to be made of AISI 316L stainless steel. The inelastic constitutive response is described through a Von Mises-Hill plasticity model with kinematic hardening. The Young's modulus is 196 GPa, the Poisson ratio is 0.3, the yield stress is 205 MPa (Auricchio et al. 2001).

The artery is modeled as a cylinder having a length of 30 mm, an internal diameter of 3 mm and a thickness of 0.5 mm. It is discretized by means of 2088 10-node tetrahedral elements with a corresponding number of nodes of 2885. To describe the mechanical behavior of the artery, a hyperelastic isotropic constitutive model along with hybrid modified elements is adopted. In particular, the constitutive equation has the following polynomial form:

$$U = C_1 \cdot (I_1 - 3) + C_2 \cdot (I_2 - 3)^3$$

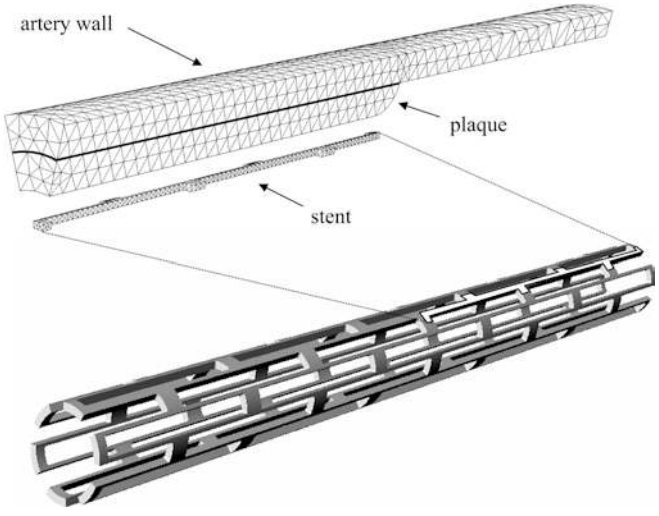

Fig. 1. Geometry and mesh of the 3-D model. It consists of three parts: the stent, the artery and the atherosclerotic plaque. Due to the model symmetries only one twelfth is reproduced in the circumferential direction and one half in the longitudinal one. A full-geometry model of the SS stent in the unexpanded configuration is reported, too. The dimensions of the stent are as follows: whole length of 16 mm, an outer diameter of 1.2 mm, a thickness of 0.1 mm, 5 slots in the longitudinal direction and 12 slots in the circumferential direction; each slot has a length of 2.88 mm. The artery has a length of 30 mm, an internal diameter of 3 mm and a thickness of 0.5 mm. The plaque has a length of 16 mm, an internal diameter of 2 mm and a thickness of 0.5 mm. It corresponds to a stenosis of 56% in terms of area reduction in the central cross section

where U is the strain energy density function, I_1 and I_2 are the first and the second invariants of the Cauchy-Green tensor (Green et al. 1968), while the coefficients C_1 and C_2 are 0.019513 and 0.02976 MPa, respectively. These two constants have been chosen such that the stress-elongation curve, depicted in Fig. 2, recalls the lowest calcified plaque reported by Salunke et al. (2001) based on biological samples.

The plaque is modeled as a cylinder (symmetric plaque) with a length of 16 mm, an internal diameter of 2 mm and a thickness of 0.5 mm. It corresponds to a stenosis of 56% in terms of area reduction in the central cross section. The plaque is discretized using 1258 10-node hybrid modified tetrahedral elements with a corresponding number of nodes of 3190, whose 593 being shared with the artery. In this case also a hyperelastic isotropic constitutive model is adopted with the following polynomial form:

$$U = C_1 \cdot (I_1 - 3) + C_2 \cdot (I_2 - 3)^2 + C_3 \cdot (I_2 - 3)^3$$

The plaque stress-elongation curve is depicted in Fig. 2 as "reference plaque" and the values of constants C_1, C_2 and C_3 are 0.04, 0.003 and 0.02976 MPa, respectively.

The mesh of the model is automatically generated by the commercial code GAMBIT (Fluent Inc., Lebanon, NH, USA). With regard to the boundary conditions, the nodes belonging to a symmetry plane are required to have zero displacement in the direction normal to the symmetry plane.

2.2
Parametric analysis

The effects of the plaque stiffness are investigated by changing the constitutive equation. If compared with the previous considered plaque, a stiffer model, simulating a calcified plaque, and a softer one, with the same constitutive equation of the artery, representing a lipidic atheroma, are developed. Figure 2 reports the three stress-elongation curves. The constitutive equation for the calcified plaque has values of the constants C_1, C_2 and C_3 equal to 0.041, 0.0031 and 0.085 MPa, respectively.

The effects of the degree of stenosis are examined by changing the plaque thickness. From the 56% of the reference model, three additional models are created. The chosen degrees of stenosis are 36% (mild stenosis), 64% (severe stenosis) and 72% (acute stenosis). For all these cases, the constitutive equation for the plaque is that adopted in the reference model.

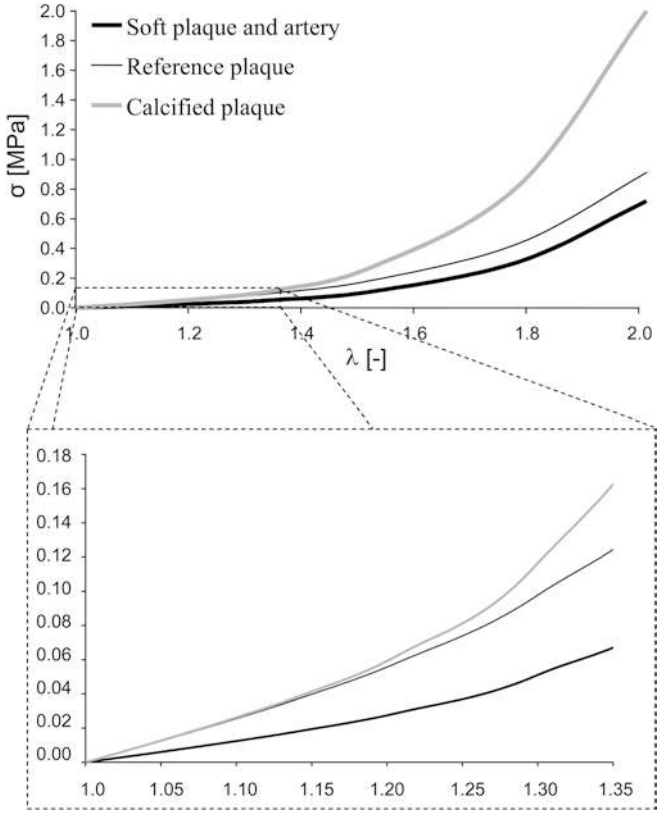

Fig. 2. Stress-elongation curves for the reference plaque, the calcified plaque and the soft plaque. The constitutive curve for the artery coincides with the soft plaque curve. In the inset an enlargement at low stress values is reported; these data show the lowest calcified plaques reported by Salunke et al. (2001)

The effects of the metal-to-artery ratio (*m/a*) are investigated by changing the geometry of the stent in terms of the actual metal surface in contact with the vascular wall (Fig. 3). From the value of 0.17 in the reference model, *m/a* is increased to 0.33 and 0.50.

Lastly, the effects of the stent material is investigated by changing the constitutive model. The classical SS plasticity model, which allows a description of the balloon-expandable stent response, is compared with the non-linear SMA model, which allows a description of the self-expandable stent response. In particular, the peculiar behavior of NiTi, the most diffused SMA, is selected. Its response depends on a thermo-elastic reversible transformation between two crystallographic structures with different physical and mechanical properties: the *austenite*, *A*, characterized by a more ordered unit cell and stable at temperatures above A_f (martensite to austenite transformation finish temperature), and the *martensite*, *M*, characterized by a less ordered unit cell and stable at temperatures below M_f (austenite to martensite transformation finish temperature) (Funakubo 1987). The self-expandable stent exploits the *pseudo-elastic effect*, that is, the SMA's unique ability to recover the original shape, once mechanically deformed, through mechanical unloading. Accordingly, the stent, in austenitic phase (A_f less than body temperature), is compressed by a protective sheath to be mounted on the catheter: during the crimping phase the material presents a nonlinear behavior due to a stress-induced conversion of austenite into martensite. When, after the insertion of the stent into the body, the sheath is retracted, a reverse transformation from martensite to austenite occurs as a result of the instability of the martensite at zero stress for temperatures higher than A_f. Accordingly, the stent expands into the artery trying to recover the original undeformed shape. Because the aim of this analysis is to compare the effects of different materials on stent performance, it is auspicial to avoid the influence of geometrical effects on the results. For this reason the dimensions of the model in the undeformed (expanded) configuration are defined so that, after compression, the SMA stent shows a geometry very similar to the undeformed configuration of the SS stent previously described: this means that the SS and SMA stents are geometrically comparable when the expansion starts. In particular the SMA stent in its expanded configuration has a length of 14 mm, an outer diameter of 3.5 mm and a thickness of 0.1 mm (Fig. 4a). The SMA stent is discretized by means of 1164 10-node hybrid modified tetrahedral elements with a corresponding number of nodes of 2577.

The NiTi peculiar constitutive behavior is described using an ad hoc developed algorithm (Auricchio and Petrini 2002) implemented into the ABAQUS/Standard code through the user subroutine UMAT. In Fig. 4b the characteristic uniaxial pseudo-elastic stress-strain curve of the material is depicted and the main parameters to be defined in the model are indicated. In the following the parameters meaning is reported:

- E is the Young modulus, assumed equal for the austenite and the martensite;
- σ_0 is the stress value indicating the mean value of the mechanical hysteresis;
- ϵ_L is the maximum transformation strain reached at the end of the austenite to martensite transformation;
- R is the measure of the mechanical hysteresis amplitude;
- σ_s is the stress threshold value at which the austenite to martensite transformation starts which depends on the temperature after the relation $\sigma_S = \sigma_0 + R$, with $\sigma_0 = \langle \beta \cdot (T - T_0) \rangle$ where β is the slope of the relation (Fig. 4c), T is the current temperature, T_0 is a reference temperature assumed equal to M_f and $\langle \bullet \rangle$indicates the positive part of the argument.

As the material mechanical characteristics of the stents are not available, medium values of a common NiTi alloy are chosen. In particular, E =70000 MPa, β =6 MPa/K, T_0= M_f=235 K, T =311 K (SMA in austenitic phase), ϵ_L=0.07, R=100 MPa.

2.3
Application to a new generation self-expandable stent

The SMA *pseudo-elasticity* of self-expandable stents offers some advantages with respect to balloon-expandable ones: a more flexible delivery system, a lower risk to overstretch the artery during

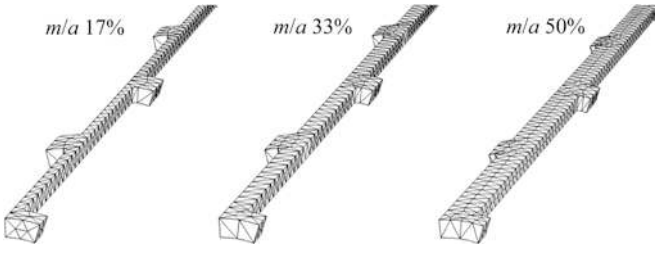

Fig. 3. CAD models of Palmaz-Schatz stents (SS stent) with different values of metal-to-artery ratio

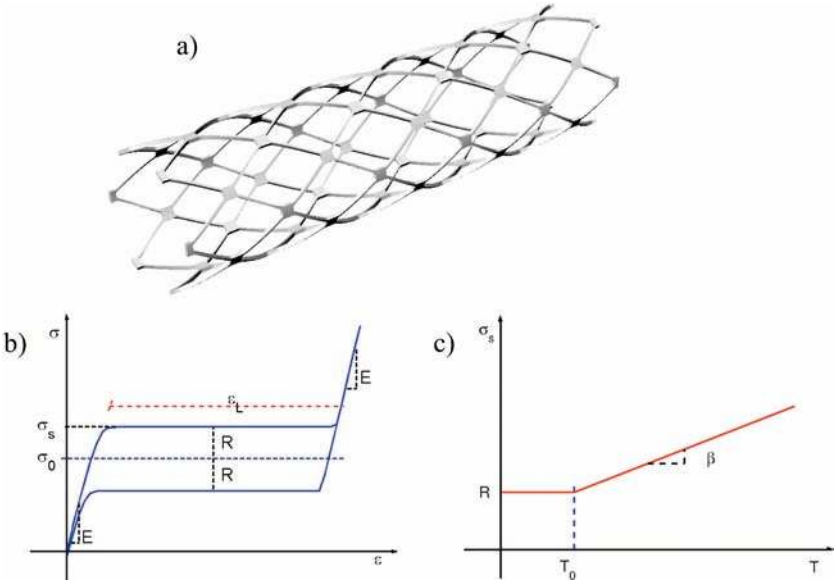

Fig. 4. a CAD model of Palmaz-Schatz stent in Nitinol (SMA stent). The length is 14 mm, the outer diameter is 3.5 mm and the thickness is 0.1 mm. **b** Characteristic uniaxial pseudo-elastic stress-strain curve. **c** Threshold transformation stress-temperature curve of the material with the main parameters used in the constitutive model indicated

expansion, lower bending stresses when deployed in tortuous vessels and the elimination, after balloon deflation, of high radial dimension reduction due to the stent elastic deformation recovery (Carter et al. 1998). Moreover, SMA, and in particular NiTi alloys, seem to have a better biocompatibility and corrosion resistance than AISI 316L (Trepanier 1999; Shih 2001; Thierry 2002). Some clinical studies (Han et al. 2001; Kobayashi et al. 2001; Taylor et al. 2001, Virmani 2002) compare NiTi alloy and stainless steel stent performance suggesting that NiTi stents, designed to allow continued expansion of the stent, induce positive remodeling of the artery, favor the long-term lumen patency and reduce the restenosis.

This observation and the lack of computational studies on NiTi stent deployment suggested to extend the numerical analyses previously described also to the case of a commercial SMA stent. In particular, a geometry very similar to the SciMED Radius stent (SciMED Live System, Maple Grove MN, USA) is considered. Its peculiar structure, with tubular-like rings, having the main function to sustain the vessel after the stent expansion, and bridging members (links), having the main function to assure the stent flexibility by allowing mutual rotation between adjacent rings, allows to study only a stent unit composed by two rings and the links between them (Petrini et al. 2004).

Artery and plaque are modeled with 6338 and 6177 3-D 10-nodes hybrid modified tetrahedral elements, respectively: a stenosis of 36% is considered. The constitutive reference model of the plaque is used. Both the extremities of the artery are constrained along the longitudinal direction to simulate the remaining part of the vessel. The stent is discretized by means of 7144 3-D 10-nodes hybrid modified tetrahedral elements with a corresponding number of nodes of 17585 (Fig. 5). The previous NiTi constitutive model is adopted. The stent rigid body motion is avoided constraining three points, positioned in the middle of the three links respectively, in the longitudinal and tangential directions.

3
Results and discussion

3.1
The stainless coronary stent expansion

Simulations for the SS coronary stent deployment are organized in different steps: 1) pre-load on the sole artery in the axial direction of 12 kPa simulating a pretensioning of 10% and pressurization of the vascular wall (including the plaque) up to 100 mmHg. During this phase the diameter of the internal plaque increases from 2 mm to 2.28 mm and the diameter of the part of the artery without the stenosis from 3 mm to 4.1 mm; 2) application of uniform linearly increasing radial pressure (P) to the internal surface of the stent so that all the nodes of the plaque are expanded at least up to a diameter of 4 mm; 3) reduction of the internal pressure on the stent until a value equal to 100 mmHg of the blood pressure. Figure 6 depicts the reference model configurations during these three steps

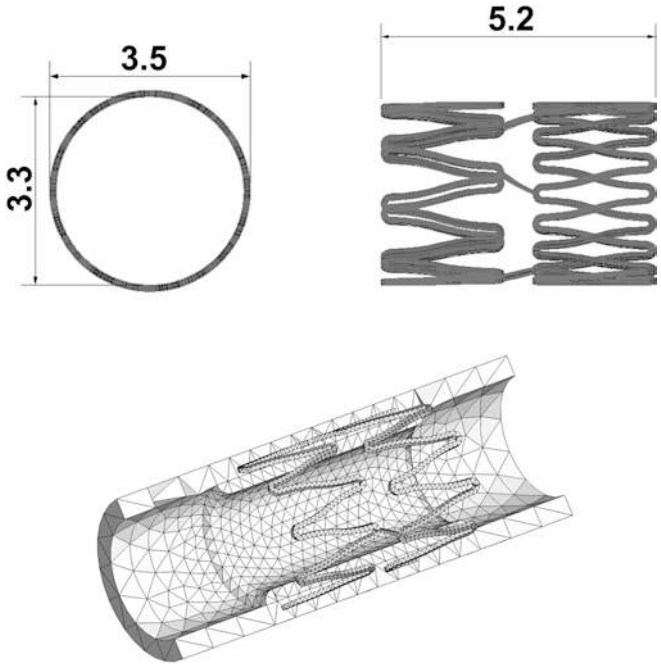

Fig. 5. CAD model of a unit of the "SciMED Radius" stent (*upper*) and entire model with artery and plaque (*lower*) for the simulation of self-expandable stent

which correspond to the following phases, respectively: 1) reaching of the in-vivo conditions in the vessel wall 2) expansion of the stent by inflation of the balloon 3) deflation of the balloon and equilibrium condition between the stent and the vessel.

Recalling that the knowledge through numerical simulations of stress variations during stent deployment can cast a new light on the mechanism of in-vivo coronary vessel response. The Von Mises stress distribution along the vessel is reported in different time-steps of the analysis in Fig. 7. In particular, the configuration of maximum expansion reached at the end of the loading phase (A), the final configuration reached at the end of the unloading phase (B) and the intermediate one (C) are considered. Configuration (C) shows, during the loading phase, a vessel diameter equal to the diameter reached after the load removal. These configurations are reported on the curve "pressure applied to the stent-plaque internal diameter" depicted in Fig. 8. The results underline how the steel elastic recovery during unloading requires a maximum expansion configuration with an overstretch of the vessel of 5.44% (point A with respect to point B in Fig. 8) and a loading addition of the 22% (point A with respect to point C in Fig. 8). Moreover, analyzing the deformed shape of the model, a non-uniform deformation of the plaque in the radial direction during the stent expansion is detectable: in particular, at the maximum pressure the plaque reaches a diameter of 4.42 mm in the zone where it is in direct contact with the device, but a diameter of 4.13 mm in the zones between the stent struts where prolapse takes place.

This type of response underlines a limit of the present model: the lack of the balloon modeling and, consequently, the simulation of its effect through the application of a pressure concentrated on the

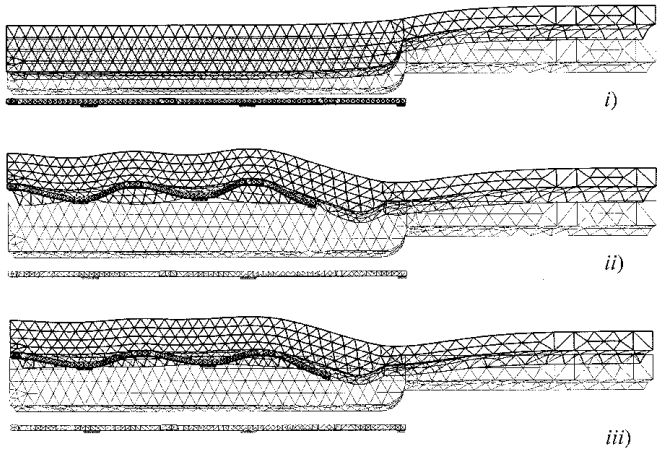

Fig. 6. Simulations of the SS coronary stent deployment. **i** Pretensioning up to 10% and pressurization of the vascular wall up to 100 mmHg. **ii** Application of uniform linearly increasing radial pressure to the internal surface of the stent so that all the nodes of the plaque are expanded at least up to a diameter of 4 mm. **iii** Reduction of the internal pressure on the stent till a value equal to 100 mmHg of the blood pressure. The undeformed configurations are depicted in *light grey*

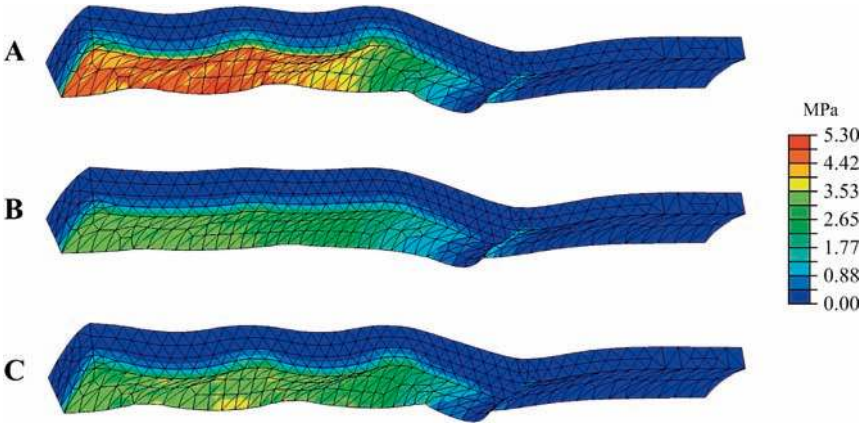

Fig. 7. Von Mises stress maps at different steps: **A** Expansion reached at the end of the loading. **B** Expansion reached at the end of the unloading. **C** Expansion reached during the loading phase when the vessel diameter is equal to the diameter at the end of the unloading

stent surface. However, we retain that this limit does not affect the results. Indeed, in the final configuration after the load removal, the prolapse disappears. In addition, comparing the intermediate (Fig. 7C) and the unloaded configuration (Fig. 7B) it is possible to verify, as expected, that the stresses on the vessel are comparable at the same internal plaque diameter. This means that during the loading phase, the stress distribution is not significantly influenced by the prolapse.

3.2
Parametric analysis

The results of the parametric analysis are reported in Fig. 9 and suggest the following:

- The plaque stiffness strongly influences the effect of the stent deployment. As it was expected, increasing the rigidity of the plaque, a higher pressure is required to open the stent (Fig. 9a), and, consequently, higher stresses are induced into the vessel.
- In the same way, increasing the degree of stenosis means more pressure is required (Fig. 9b) and higher stresses are induced.
- On the contrary, increasing the metal-to-artery ratio means lower pressure is required (Fig. 9c) and lower stresses are induced.

To compare the effects of stent different materials onto the vessel wall mechanical stress state, we performed simulations for the SMA superelastic coronary stent deployment organized in the following

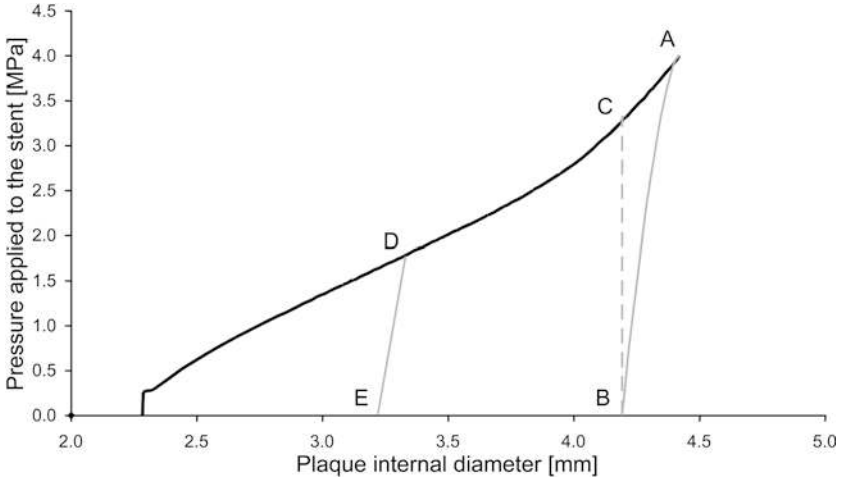

Fig. 8. Pressure applied to the stent—plaque internal diameter curve from the SS expansion numerical simulation. The following points can be recognized: **A** Configuration of maximum load, **B** corresponding configuration after unloading. **C** Configuration during loading having the same diameter as B. **D** Configuration that must be reached to obtain unloading the same diameter as E. **E** Configuration corresponding to that reached with the SMA stent

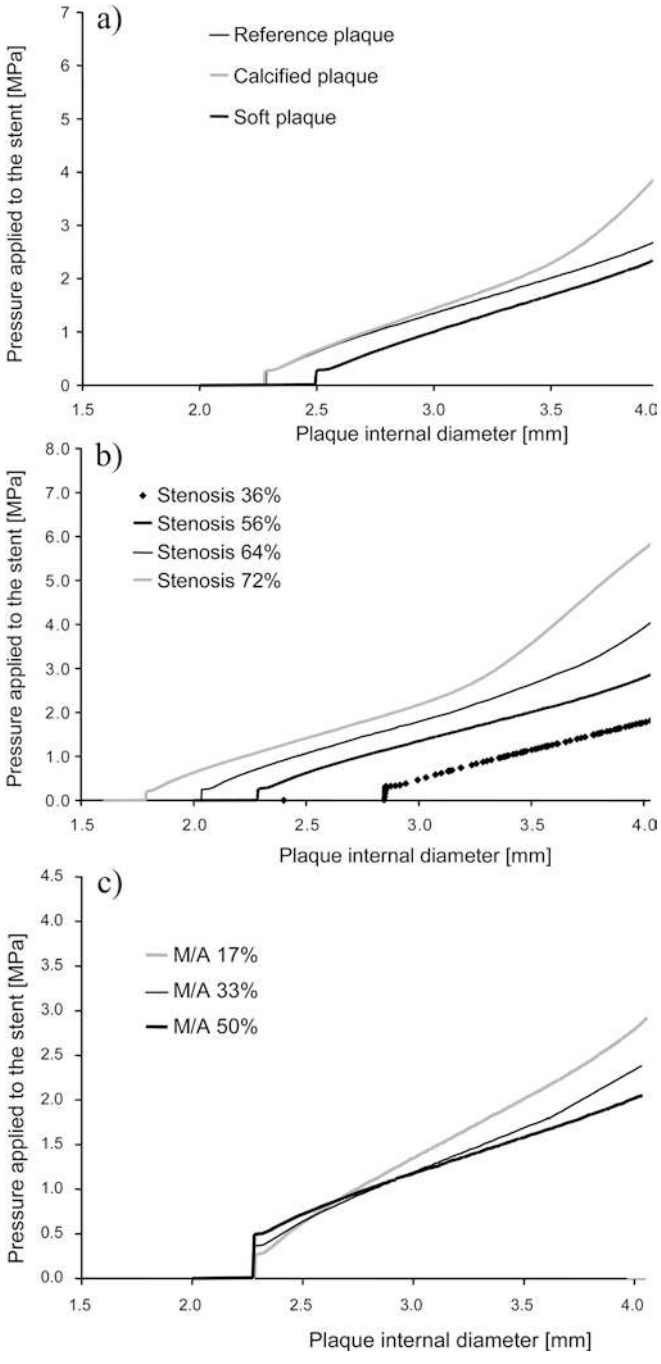

Fig. 9. Pressure applied to the stent–plaque internal diameter curve from the parametric analyses performed on the SS stent considering the following cases: **a** Different stiffness of the plaque. **b** Different degree of stenosis. **c** Different metal-to-artery ratio

steps: 1) Pretensioning up to 10% and pressurization of the vascular wall (100 mmHg). In this stage the stent maintains the undeformed original configuration with a diameter larger than the stenosis, being the contact not activated. 2) Crimping of the stent. Under radial displacement control the stent internal diameter is reduced of the 42%. 3) Releasing and self-expansion of the stent after removal of the displacement constraints and activation of the contact option. 4) Application of the pressure on the internal surface of the stent until a value equal to 100 mmHg simulating the blood pressure.

At the end of the expansion, when the equilibrium between the expanding force of the stent and the reacting force of the vessel is reached, the stent enlarges the vessel up to an internal diameter of 3.2 mm. In Fig. 10 (upper part) the Von Mises stresses at the maximum expansion are depicted. The stent induces an increasing state of stress uniform along the vessel, but it is not able to recover completely the original shape (undeformed diameter equal to 3.5 mm). On one hand, because the expansion derives from intrinsic properties of the material, superelastic stent does not require an overexpansion of the vessel as in the case of SS and hence it induces lower stress and lower damage in the vessel. This is evident if we extrapolate from the curve of Fig. 8 the configuration of maximum

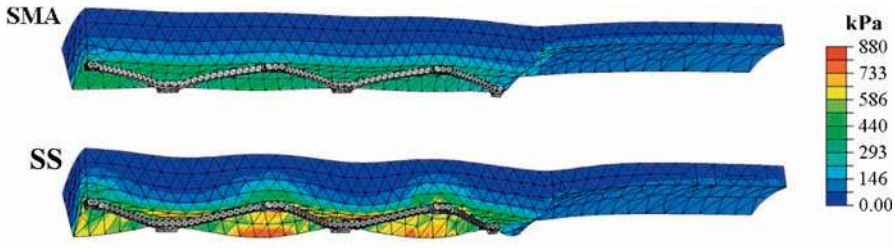

Fig. 10. Von Mises stress maps with an expanded internal vessel diameter of 3.2 mm for the self-expandable SMA stent (*top*) and the SS stent (*bottom*)

expansion (point D), which has to be reached by the SS stent to have, after unloading, the same effect on the vessel as the SMA stent (point E). Figure 10 (lower part) depicts the deformed model when the SS stent has reached the configuration corresponding to point D. The Von Mises stresses reach values 50% higher than those induced by SMA stent (upper part of Fig. 10). On the other hand, superelastic stent behavior and efficacy depend strictly on the material mechanical characteristics. Accordingly, as it results from the simulation, the lower stiffness of the SMA induces a lower capability to expand and to contrast the vessel elastic recoil. This is confirmed by the manufacturers who suggest performing an angioplasty prior/after the stenting. The inflation of a balloon into the stenotic vessel produces fractures in the plaque, reducing its stiffness. Our model is not able to describe this phenomenon and hence it overestimates the radial recoil of the vessel.

3.3
Application to a new generation self-expandable stent

The analyses performed on the SciMED Radius unit design confirm the last observation: also in this case the chosen material parameters make the stent unable to re-open the artery completely. On the other hand, the geometry of the SciMED Radius shows a better performance. This becomes evident observing that at the same percentage of crimping (42%) the Palmaz-Schatz stent shows higher and more concentrated maximum strain (Fig. 11). This means that a small percentage of material exploits pseudo-elasticity with higher risk of overcoming maximum recoverable strain limit.

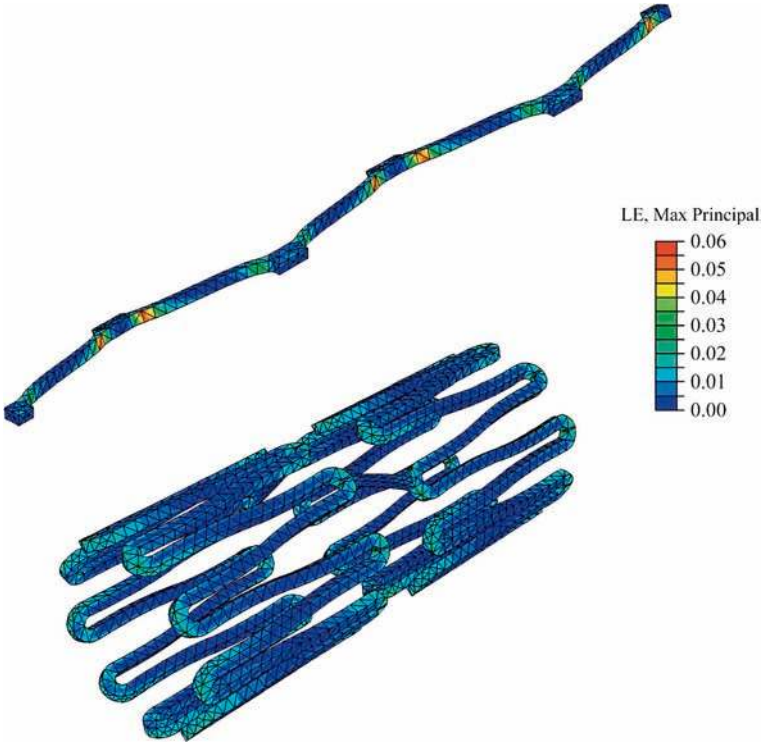

Fig. 11. Maximum principal strain maps for the NiTi Palmaz-Schatz and SciMED Radius stents at the maximum percentage of crimping (42%)

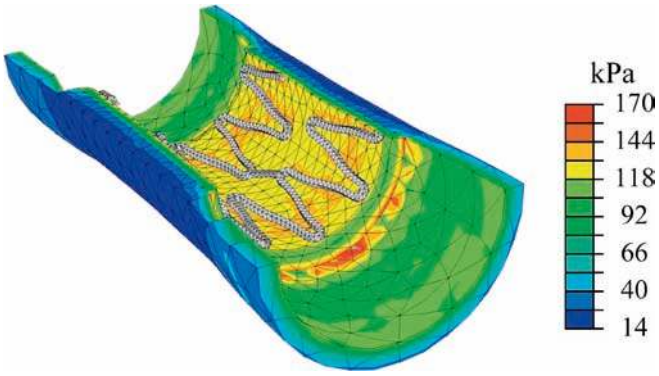

Fig. 12. Von Mises stresses distribution induced on the vessel by the self-expansion of the SciMED Radius SMA stent

Comparing the stress distribution generated by the expansion of the SciMED Radius (Fig. 12) and that by the SMA Palmaz-Schatz stent in a 36% stenotic vessel, the former induces lower stresses on the vessel (maximum von Mises stress 170 vs 280 kPa).

Finally, the results of this analysis show how the computational methodology herewith proposed can be easily applied also to new generation coronary stents and can be useful to develop comparative studies between different types of devices.

3.4 Limitations

The effects of vessel curvature have not been taken into consideration. This surely has effects on the restenosis phenomenon. Indeed, the straightening induced by the stiffness of the stent is a predictor for major adverse cardiac events and angiographic restenosis as observed in the study by Gyongyosi et al. (2000).

As regards the artery and the plaque, the absence of residual stress, of wall anisotropy and of artery heterogeneity (media versus adventitia) are additional limitations. This last assumption is, however, acceptable for the artery if we consider that the adventitia serves primarily as a thin protective sheath against acute over distension in the presence of large pressure (Stergiopulos et al. 2001). Furthermore, our models consider only a simplified symmetric geometry of the plaque.

The absence of any balloon modeling for the SS models is an imperfection of this study. The effects of the balloon expansion have been simulated with a uniform pressure, as reported also by Doumulin and Cochelin (2000), applied directly on the internal metallic surface of the stent through follower loads.

Furthermore, modeling of the plaque rupture mechanism has not been addressed in this study. Fracture and/or micro-damage as well as damage to the arterial wall as the stent is deployed would change the mechanical properties of the vascular wall in terms of loss of stiffness. It is not clear at what level of stress the plaque fractures; some experimental results (Salunke et al. 2001) showed compressive rupture at low levels (250–600 kPa) if compared with those of the inflating pressure (0.8–1 MPa). It should, however, be considered that the balloon carries much of the load. In the literature the computational studies simulating the angioplastic or stenting procedure did not take into account any rupture mechanism, a part from a work by Oh and colleagues (1994) who considered a failure criterion for the plaque regarding the fracture at the plaque-artery junction site, which is, however, not based on experimental data.

Lastly, in regards to the application of this methodology to the new generation of SMA stents, because of the strong dependency of the material properties from the alloy composition and thermo-mechanical treatment, the present study does not make any attempt to give quantitative indications, but shows the FEM potentials to also study new generation NiTi stent performance. The exact knowledge of the thermo-mechanical properties should surely add values to the results herewith proposed.

References

Auricchio, F.; Petrini, L.: Improvements and algorithmical considerations on a recent three-dimensional model describing stress-induced solid phase transformations. Int J Num Meth Eng 55 (2002) 1255–1284

Auricchio, F.; Di Loreto, M.; Sacco, E.: Finite-element analysis of a stenotic revascularization through a stent insertion. Comput Meth Biomech Biomed Eng 4 (2001) 249–264

Bassiouny, H.S.; Zarins, C.K.; Kadowaki, M.H.; Glagov, S.: Hemodynamic stress and experimental aortoiliac atherosclerosis. J Vasc Surg 19 (1994) 426–434

Carter, A.J.; Scott, D.; Laird, J.R.; Bailey, L.; Kovach, J.A.; Hoopes, T.G.; Pierce, K.; Heath, K.; Hess, K.; Farb, A.; Virmani, R.: Progressive vascular remodeling and reduced neointimal formation after placement of a thermoelastic self-expanding nitinol stent in an experimental model. Cathet Cardiovasc Diagn 44 (1998) 193-201

Degertekin, M.; Regar, E.; Tanabe, K.; Lemos, P.; Lee, C.H.; Smits, P.; de Feyter, P.; Bruining, N.; Sousa, E.; Abizaid, A.; Ligthart, J.; Serruys, P.W.: Evaluation of coronary remodeling after sirolimus-eluting stent implantation by serial three-dimensional intravascular ultrasound. Am J Cardiol 91 (2003) 1046–1050

Dumoulin, C.; Cochelin, B.: Mechanical behaviour modelling of balloon-expandable stents. J Biomech 33 (2000) 1461–1470

Edelman, E.R.; Rogers, C.: Pathobiologic response to stenting. Am J Cardiol 81(7A) (1998) 4E-6E

Feldman, C.L.; Stone, P.H.: Intravascular hemodynamic factors responsible for progression of coronary atherosclerosis and development of vulnerable plaque. Curr Opin Cardiol 15 (2000) 430–440

Funakubo, H.: Shape memory alloys. Taylor & Francis, London (1987)

Gibson, C.M.; Diaz, L.; Kandarpa, K.; Sacks, F.M.; Pasternak, R.C.; Sandor, T.; Feldman, C.; Stone, P.H.: Relation of vessel wall shear stress to atherosclerosis progression in human coronary arteries. Arterioscler Thromb 13 (1993) 310–315

Gnasso, A.; Irace, C.; Carallo, C.; De Franceschi, M.S.; Motti, C.; Mattioli, P.L.; Pujia, A.: In vivo association between low wall shear stress and plaque in subjects with asymmetrical carotid atherosclerosis. Stroke 28 (1997) 993–998

Gourisankaran, V.; Sharma, M.G.: The finite-element analysis of stresses in atherosclerotic arteries during balloon angioplasty. Crit Rev Biomed Eng 28 (2000) 47–51

Green, A.E.; Zerna, W.: Theoretical Elasticity. Clarendon Press, Oxford (1968)

Gyongyosi, M.; Yang, P.; Khorsand, A.; Glogar, D.: Longitudinal straightening effect of stents is an additional predictor for major adverse cardiac events. Austrian Wiktor Stent Study Group and European Paragon Stent Investigators. J Am Coll Cardiol 35 (2000) 1580–1589

Han, R.O.; Schwartz, R.S.; Kobayashi, Y.; Wilson, S.H.; Mann, J.T.; Sketch, M.H.; Safian, R.D.; Lansky, A.; Popma, J.; Fitzgerald, P.J.; Palacios, I.F.; Chazin-Caldie, M.; Goldberg, S.: Comparison of self-expanding and balloon-expandable stents for the reduction of restenosis. Am J Cardiol 88 (2001) 253–259

Holzapfel, G.A.; Stadler, M.; Schulze-Bauer, C.A.J.: A Layer-Specific Three-Dimensional Model for the Simulation of Balloon Angioplasty using Magnetic Resonance Imaging and Mechanical Testing. Ann Biomed Eng 30 (2002) 753–767

Jiang, Y.; Kohara, K.; Hiwada, K.: Low wall shear stress contributes to atherosclerosis of the carotid artery in hypertensive patients. Hypertens Res 22 (1999) 203–207

Jiang, Y.; Kohara, K.; Hiwada, K.: Association between risk factors for atherosclerosis and mechanical forces in carotid artery. Stroke 31 (2000) 2319–2324

Kobayashi, Y.; Honda, Y.; Christie, G.L.; Teirstein, P.S.; Bailey, S.R.; Brown, C.L. III; Matthews, R.V.; De Franco, A.C.; Schwartz, R.S.; Goldberg, S.; Popma, J.J.; Yock, P.; Fitzgerald, P.J.: Long-term vessel response to a self-expanding coronary stent: a serial volumetric intravascular ultrasound analysis from the ASSURE trial. J Am Coll Cardiol 37 (2001) 1329–1334

Lee, R.T.; Loree, H.M.; Cheng, G.C.; Lieberman, E.H.; Jaramillo, N.; Schoen, F.J.: Computational structural analysis based on intravascular ultrasound imaging before in vitro angioplasty: Prediction of plaque fracture locations. J Am Coll Cardiol 21 (1993) 777–782

Leon, M.; Teirstein, P.; Moses, J.; Tripuraneni, P.; Lansky, A.J.; Jani, S.; Wong, S.C.; Fish, D.; Ellis, S.; Holmes, D.R.; Kerieakes, D.; Kuntz, R.E.: Localized intracoronary gamma radiation therapy to inhibit the recurrence of restenosis after stenting (GAMMA-1). N Engl J Med 344 (2001) 250–256

Migliavacca, F.; Petrini, L.; Colombo, M.; Auricchio, F.; Pietrabissa, R.: Mechanical behavior of coronary stents investigated through the finite element method. J Biomech 35 (2002) 803–811

Mintz, G.S.; Kent, K.M.; Pichard, A.D.; Satler, L.F.; Popma, J.J.; Leon, M.B.: Contribution of inadequate arterial remodeling to the development of focal coronary artery stenoses. An intravascular ultrasound study. Circulation 95 (1997) 1791–1798

Moore, J.E.; Berry, J.L.: Fluid and solid mechanical implications of vascular stenting. Ann Biomed Eng 30 (2002) 498–508

Morice, M.C.; Surruys, P.W.; Sousa, J.E.; Fajadet, J.; Ban Hayashi, E.; Perin, M.; Colombo, A.; Schuler, G.; Barragan, P.; Guagliumi, G.; Molnar, F.; Falotico.: A Randomized comparison of a sirolimus-eluting stent with a standard stent for coronary revascularization. N Engl J Med 346 (2002) 1773–1780

Oh, S.; Kleinberger, M.; McElhaney, J.H.: Finite-element analysis of balloon angioplasty. Med Biol Eng Comput 32 (1994) S108–S114

Petrini, L.; Migliavacca, F.; Dubini, G.; Auricchio, F.: Numerical investigation of the intravascular coronary stent flexibility. J Biomechanics 37 (2004) 495–504

Popma, J.J.; Suntharalingam, M.; Lansky, A.J.; Heuser, R.R.; Speiser, B.; Teirstein, P.S.; Massullo, V.; Bass, T.; Henderson, R.; Silber, S.; von Rottkay, P.; Bonan, R.; Ho, K.K.; Osattin, A.; Kuntz, R.E.: Randomized trial of 90Sr/90Y beta-radiation versus placebo control for treatment of in-stent restenosis (START). Circulation 106 (2002) 1090–1096

Prendergast, P.J.; Lally, C.; Daly, S.; Reid, A.J.; Lee, T.C.; Quinn, D.; Dolan, F.: Analysis of prolapse in cardiovascular stents: a constitutive equation for vascular tissue and finite element modelling. J Biomech Eng 125 (2003) 692–699

Rogers, C.; Tseng, D.Y.; Squere, J.C.; Edelman, E.R.: Balloon-artery interactions during stent placement. A finite element analysis approach to pressure, compliance, and stent design as contributors to vascular injury. Circ Res 84 (1999) 378–383

Salunke, N.V.; Topoleski, L.D.T.; Humphrey, J.D.; Mergner, W.J.: Compressive stress-relaxation of human atherosclerotic plaque. J Biomed Mater Res 55 (2001) 236–241

Sangiorgi, G.; Taylor, A.J.; Farb, A.; Carter, A.J.; Edwards, W.D.; Holmes, D.R.; Schwartz, R.S.; Virmani, R.: Histopathology of postpercutaneous trans-luminal coronary angioplasty remodeling in human coronary arteries. Am Heart J 138 (1999) 681–687

Saul, G.D.: Arterial stress from intraluminal pressure modified by tissue pressure offers a complete explanation for the distribution of atherosclerosis. Med Hypotheses 52 (1999) 349–351

Schwartz, R.S.; Topol, E.J.; Serruys, P.W.; Sangiorgi, G.; Holmes, D.R. Jr: Artery size, neointima, and remodeling: time for some standards. J Am Coll Cardiol 32 (1998) 2087–2094

Schwartz, R.S.; Henry, T.D.: Pathophysiology of coronary artery restenosis. Rev Cardiovasc Med 3 Suppl 5 (2002) S4-S9

Shih, C.C.; Shih, C.M.; Chen, Y.L.; Su, Y.Y.; Shih, J.S.; Kwok, C.F.; Lin, S.J.: Growth inhibition of cultured smooth muscle cells by corrosion products of 316 L stainless steel wire. J Biomed Mater Res 57 (2001) 200–207

Sousa, J.E.; Costa, M.A.; Abizaid, A.C.; Rensing, B.J.; Abizaid, A.S.; Tanajura, L.F.; Kozuma, K.; Van Langenhove, G.; Sousa, A.G.; Falotico, R.; Jaeger, J.; Popma, J.J.; Serruys, P.W.: Sustained suppression of neointimal proliferation by sirolimus-eluting stents: one-year angiographic and intravascular ultrasound follow-up. Circulation 104 (2001) 2007–2011

Stergiopulos, N.; Vulliemoz, S.; Rachev, A.; Meister, J.-J.; Greenwald, S.E. : Assessing the homogeneity of the elastic properties and composition of the pig aortic media. J Vasc Res 38 (2001) 237–246

Taylor, A.J.; Gorman, P.D.; Kenwood, B.; Hudak, C.; Tashko, G.; Virmani, R.: A comparison of four stent designs on arterial injury, cellular proliferation, neointima formation, and arterial dimensions in an experimental porcine model. Cathet Cardiovasc Intervent 53 (2001) 420–425

Thierry, B.; Merhi, Y.; Bilodeau, L.; Trepanier, C.; Tabrizian, M.: Nitinol versus stainless steel stents: acute thrombogenicity study in an ex vivo porcine model. Biomaterials 23 (2002) 2997–3005

Thubrikar, M.J.; Robicsek, F.: Pressure-induced arterial wall stress and atherosclerosis. Ann Thorac Surg 59 (1995) 1594–1603

Trepanier, C.; Leung, T.K.; Tabrizian, M.; Yahia, L.H.; Bienvenu, J.G.; Tanguay, J.F.; Piron, D.L.; Bilodeau, L.: Preliminary investigation of the effects of surface treatments on biological response to shape memory NiTi stents. J Biomed Mater Res 48 (1999) 165–171

Virmani, R.: Self-expanding stent deployment strategies may be the key to reducing in-stent restenosis. Catheter Cardiovasc Interv 56 (2002) 487–488

Waksman, R.; Raizner, A.E.; Yeung, A.C.; Lansky, A.J.; Vandertie, L.: Use of localised intracoronary beta radiation in treatment of in-stent restenosis: The INHIBIT randomised controlled trial. Lancet 359 (2002) 543–544

Welt, F.G.; Rogers, C.: Inflammation and restenosis in the stent era. Arterioscler Thromb Vasc Biol 22 (2002) 1769–1776

Wentzel, J.J.; Gijsen, F.J.; Stergiopulos, N.; Serruys, P.W.; Slager, C.J.; Krams, R.: Shear stress, vascular remodeling and neointimal formation. J Biomech 36 (2003) 681–688

Zarins, C.K.; Giddens, D.P.; Bharadvaj, B.K.; Sottiurai, V.S.; Mabon, R.F.; Glagov, S.: Carotid bifurcation atherosclerosis. Quantitative correlation of plaque localization with flow velocity profiles and wall shear stress. Circ Res 53 (1983) 502–514